TOXICOLOGICAL SCIENCES **101(2)**, 239–253 (2008)
doi:10.1093/toxsci/kfm240
Advance Access publication September 13, 2007

Characterization of Nanomaterial Dispersion in Solution Prior to *In Vitro* Exposure Using Dynamic Light Scattering Technique

Richard C. Murdock, Laura Braydich-Stolle, Amanda M. Schrand, John J. Schlager, and Saber M. Hussain[1]

Applied Biotechnology Branch, Human Effectiveness Directorate Air Force Research Laboratory/HEPB, Wright-Patterson Air Force Board, Ohio 45433

Received June 1, 2007; accepted August 23, 2007

The need to characterize nanoparticles in solution before assessing the *in vitro* toxicity is a high priority. Particle size, size distribution, particle morphology, particle composition, surface area, surface chemistry, and particle reactivity in solution are important factors which need to be defined to accurately assess nanoparticle toxicity. Currently, there are no well-defined techniques for characterization of wet nanomaterials in aqueous or biological solutions. Previously reported nanoparticle characterization techniques in aqueous or biological solutions have consisted of the use of ultra-high illumination light microscopy and disc centrifuge sedimentation; however, these techniques are limited by the measurement size range. The current study focuses on characterizing a wide range of nanomaterials using dynamic light scattering (DLS) and transmission electron microscopy, including metals, metal oxides, and carbon-based materials, in water and cell culture media, with and without serum. Cell viability and cell morphology studies were conducted in conjunction with DLS experiments to evaluate toxicological effects from observed agglomeration changes in the presence or absence of serum in cell culture media. Observations of material-specific surface properties were also recorded. It was also necessary to characterize the impact of sonication, which is implemented to aid in particle dispersion and solution mixture. Additionally, a stock solution of nanomaterials used for toxicology studies was analyzed for changes in agglomeration and zeta potential of the material over time. In summary, our results demonstrate that many metal and metal oxide nanomaterials agglomerate in solution and that depending upon the solution particle agglomeration is either agitated or mitigated. Corresponding toxicity data revealed that the addition of serum to cell culture media can, in some cases, have a significant effect on particle toxicity possibly due to changes in agglomeration or surface chemistry. It was also observed that sonication slightly reduces agglomeration and has minimal effect on particle surface charge. Finally, the stock solution experienced significant changes in particle agglomeration and surface charge over time.

Key Words: **dynamic light scattering; nanomaterials; toxicity; characterization.**

Currently, the field of nanotechnology is growing at an exponential rate and nanomaterials are being incorporated into all aspects of life. Nanomaterials, by definition, have one dimension that falls into the 1–100 nm range, with the nanomaterials typically comprising metal or carbon (The Royal Society, 2004). In medicine, proposed uses for nanomaterials include drug delivery, imaging, and the formation of bone composites (Kim *et al*., 2001; Murugan and Ramakrishna, 2005; Sinha and Trehan, 2003; Wu *et al*. 2005). Furthermore, companies in the food and cosmetics industries have incorporated nanomaterials to enhance the quality of their products (Kimbrell, 2006). Lastly, defense and engineering scientists have shown that nanomaterials are potentially useful in electronics, sensors, munitions, and energetic/reactive systems involved with the advancement of propulsion technology (Ringer and Ratinac, 2004).

In recent years, it has become evident that it is necessary to systematically and accurately define particle characteristics in order to understand the potential toxicity of nanoparticles to biological systems to ensure that results are reproducible (Hood, 2004; The Royal Society, 2004). Nanoparticle affects on biological activity are unknown at this point; therefore, accurate characterization of these materials is essential to provide the basis for understanding the properties of nanoparticles that determine their biological effects (Powers *et al*., 2006). There are unique properties that lend themselves to nanomaterials and differentiate them from their bulk counterparts. However, the burden of testing the same parameters for bulk materials before conducting a nanotoxicity study would be overwhelming and costly to researchers. Therefore, certain characteristics have been identified which must be considered for the characterization of nanomaterials prior to study and these properties are size, shape, dispersion, physical and chemical properties, surface area, and surface chemistry (Bucher *et al*., 2004; Oberdorster *et al*., 2005a,b; Powers *et al*., 2006). Many of these properties can be evaluated using dry, powdered nanomaterials; however, it is unknown if nanomaterials retain the same nanoproperties once in biologically relevant solutions. This is a critical question that must be addressed because once introduced into the body, the nanomaterials will come in contact with, and potentially

[1] To whom correspondence should be addressed at Air Force Research Laboratory Building 837, ''R'' Street, Area B Wright-Patterson Air Force Board, OH 45433-5707. Fax: (937) 904-9610. E-mail: saber.hussain@wpafb.af.mil.

become dispersed in, a variety of bodily fluids. Wallace *et al*. (2007) showed that nanoparticulates from combustion processes can adsorb components of lung surfactant, altering the surface chemistry of the particle; however, there was little characterization of particle composition or particle size in the surfactant. Furthermore, in some cases, *in vitro* testing is used to determine the predictive toxicity of nanomaterials before proceeding with *in vivo* studies, and the nanomaterials must be optimally dispersed in order to uniformly dose the cells.

Powers *et al*. (2006) reviewed the different methods of nanomaterial characterization and proposed dynamic light scattering (DLS) as a useful technique to evaluate particle size, size distribution, and the zeta potential of nanomaterials in solution. DLS has been used in recent and past studies, as early as 1975, as a simple method for analyzing suspension stability and measurement of particle size in solution (Berne and Pecora, 1975; Simakov and Tsur, 2006; Williams *et al*., 2006; Wu *et al*., 2005).

The present study used DLS, in conjunction with transmission electron microscopy (TEM), to evaluate the size distribution, state of dispersion, and zeta potential for a variety of nanomaterials that had been dispersed in water and dosing media prior to *in vitro* toxicology experiments. Metal and metal oxide nanoparticles, such as aluminum, aluminum oxide, copper, silicon dioxide, titanium dioxide, and silver, as well as carbon-based nanomaterials, such as carbon nanotubes (CNT) and carbon black (CB), were evaluated. It has been observed that dispersion of nanomaterials in solution rarely leads to distribution at the primary particle size. This agglomeration raises concerns when considering size-dependent toxicity, specific surface area toxicity, and dose-dependent toxicity for *in vitro* experiments. For this reason, parallel cell viability assays and cell morphology studies were conducted on select nanomaterials to observe toxicity differences with and without the presence of serum in cell culture media. Observations were made about each particles surface characteristics as well to possibly correlate toxicity data.

One method used in our research to decrease agglomeration in solution is to use mechanical agitation such as sonication. Probe sonication was studied to determine its impact on the particle characteristics, such as average agglomerate size, polydispersity of the solution, and surface charge. In addition, there is increasing concern that stock solutions of nanomaterials for nanotoxicity experiments can change over time, perhaps impacting the results of multiple toxicity studies. Therefore, in the present study, we examined stock solutions of Cu nanoparticles over a period of approximately 1 month.

MATERIALS AND METHODS

Chemicals. Aluminum oxide (Al_2O_3) nanoparticles (30 and 40 nm), aluminum (Al) nanoparticles (50, 80, and 120 nm), hydrocarbon-coated silver (HC-Ag) nanoparticles (15, 25, and 80 nm), and copper (Cu) nanoparticles (40, 60, and 80 nm) were synthesized and generously received in powder form from Dr Karl Martin of NovaCentrix, Austin, TX (formerly Nanotechnologies, Inc.). Polysaccharide-coated silver (PS-Ag) nanoparticles (10, 25–30, and 80 nm) were received dispersed in deionized water (DI H_2O) from Dr Dan Goia's Laboratory at Clarkson University, Potsdam, NY. Titanium dioxide (TiO_2) nanoparticles of 39 nm (100% anatase), 39 nm (61% anatase, 31% rutile), 39 nm (40% anatase, 60% rutile), and 40 nm (amorphous) sizes as well as the 5, 10, 16, 50, and 100 nm (all 100% anatase) sizes were generously provided by Dr Pratim Biswas' group in the Department of Chemical Engineering Washington University in St Louis. Silicon dioxide (SiO_2) nanoparticles (51, 110, and 420 nm) and the silicon dioxide–coated fluorophores (SiO_2-Fluorescein Isothiocyanate (FITC), SiO_2-Rhodamine B (RB)), ~73 nm size, were provided by Dr Baohua Gu from the Oak Ridge National Laboratories, Oak Ridge, TN. CNT, single-walled carbon nanotubes (SWNT), commercial multiwalled carbon nanotubes, and carboxyl functionalized multiwalled carbon nanotubes (MWNT-COOH) were received from Dr Liming Dai at the University of Dayton, Dayton, OH and produced via methods described in Dai et al., 2005. Nanometer-sized CB (30 nm) particles were received from the Cabot Corporation, Alpharetta, GA. Ham's nutrient mixture F-12 media (Kaighn's modified), RPMI-1640 media, heat-inactivated fetal bovine serum (HI-FBS), and HI-horse serum were purchased from American Type Culture Collection, Manassas, VA. The Dulbecco's modified Eagle's medium (DMEM)/F-12 media, normal FBS, and penicillin/streptomycin (pen/strep) were purchased from Sigma Chemical Company, St Louis, MO.

Sample particles stock solution and media preparation. Nanomaterials received in dry powder form (Al_2O_3, Al, Ag, HC-Ag, Cu, SiO_2, and TiO_2) were weighed on an analytical mass balance, suspended in deionized water at a concentration of 1 mg/ml, and then probe sonicated for 30 s at 35–40 W to aid in mixing and forming a homogeneous dispersion. Nanoparticles received which were already dispersed in water (PS-Ag) were diluted from bulk concentrations to 1 mg/ml working stock concentrations and were also sonicated for 30 s at 35 W. Sonication of the samples was only performed initially to aid in dispersion with the exception of the time course sonication study. For size measurement trials, the 1 mg/ml nanoparticle stock solutions were then used to make 25–50 μg/ml solutions in water, cell culture media only, and/or cell culture media with serum (Table 1 shows the samples made for each particle measured and their concentrations at the time of measurement). As a note, the type of media chosen for dispersion of a particular particle coincided with current *in vitro* toxicology studies. The RPMI-1640 media with serum was supplemented with 10% HI-FBS, 10% HI-horse serum, and 1% pen/strep. The RPMI-1640 media without serum had only 1% pen/strep added. The F-12K media with serum added contained either 10% FBS or 20% FBS (as labeled) with 1% pen/strep, while the F-12K without serum contained only 1% pen/strep. The DMEM/F-12 media with serum consisted of 10% HI-FBS and 1% pen/strep, while the DMEM/F-12 media without serum was supplemented with only 1% pen/strep.

TEM of nanoparticles. TEM characterization was performed to obtain nanoparticle size and morphology on a Hitachi H-7600 tungsten-tip instrument at an accelerating voltage of 100 kV. Nanoparticles were examined after suspension in water and subsequent deposition onto formvar/carbon-coated TEM grids. The AMT software for the digital TEM camera was calibrated for size measurements of the nanoparticles. Information on mean size and SD was calculated from measuring over 100 nanoparticles in random fields of view in addition to images that show general morphology of the nanoparticles.

X-ray photoelectron spectroscopy. X-ray photoelectron spectroscopy (XPS) characterization was performed to detect surface chemical composition on a Surface Science Labs SSX-100 system. This instrument has a monochromatic aluminum x-ray source with a nominal x-ray beam diameter of 600 μm. The Al K (alpha) x-ray energy used was 1486.6 eV. To generate these x-rays, an aluminum anode is bombarded by an electron gun operating at 10 kV with 10 mA emission current. The x-rays strike the sample causing photons at characteristic energy levels (different for each element) to be emitted. Sample preparation consisted of placing a drop of the Ag nanoparticle sample in water

TABLE 1
Parameters for DLS/LDV Measurement for Various Nanomaterials

Particles	Solvents used	Concentration (μg/ml)
Al_2O_3 (30 nm, 40 nm)	DI H_2O, RPMI-1640, RPMI-1640 with 10% FBS (HI), and 10% horse serum (HI)	50
Al (80 nm, 120 nm)	DI H_2O, F-12K, F-12K with 10% FBS (HI), F-12K with 20% FBS (HI)	25
Hydrocarbon-coated Ag, (15 nm, 25 nm); uncoated Ag, (80 nm); polysaccharide-coated Ag, (10, 25–30, 80 nm)	DI H_2O, RPMI-1640, RPMI-1640 with 10% FBS (HI), and 10% horse serum (HI)	25
Cu (40, 60, 80 nm)	DI H_2O, RPMI-1640, RPMI-1640 with 10% FBS (HI), and 10% horse serum (HI)	25
SiO_2, (35, 51, 110, 420 nm), SiO_2-FITC (73 nm), SiO_2-RB, (73 nm)	DI H_2O, DMEM/F-12	50
TiO_2 (39 nm 100% anatase, 39 nm 61% anatase 39% rutile, 39 nm 40% anatase 60% rutile, 40 nm amorphous, 5, 10, 16, 50, 100 nm)	DI H_2O, DMEM/F-12, DMEM/F-12 with 10% FBS (HI)	50
CNT (SWNT, MWNT, MWNT-COOH, CNT)	DI H_2O	50
CB, (CB ~30 nm)	DI H_2O, DMEM/F-12, DMEM/F-12 with 10% FBS (HI)	25

on a piece of clean Al foil and then allowing the water to evaporate at room temperature before measurements.

DLS and laser Doppler velocimetry of nanoparticles in solution. DLS and laser Doppler velocimetry (LDV), for characterization of size and zeta potential of the nanoparticles in solution, were performed on a Malvern Instruments Zetasizer Nano-ZS instrument. DLS analyzes the velocity distribution of particle movement by measuring dynamic fluctuations of light scattering intensity caused by the Brownian motion of the particle. This technique yields a hydrodynamic radius, or diameter, to be calculated via the Stokes-Einstein equation from the aforementioned measurements. It yields an overall measurement of the particle perpendicular to the light source at that instant. The measurement technique used by the Zetasizer Nano-ZS to measure the zeta potential of particles in a solution is known as LDV. This technique uses a laser, which is being passed through the sample, to measure the velocity of the particles in an applied electric field of a known value which is known as electrophoretic mobility. The device uses a 4-mW He-Ne 633 nm laser to analyze the samples as well as an electric field generator (for LDV measurements). Samples were prepared as previously described in Sample Particles Stock Solution and Media Preparation section, vortexed to provide a homogeneous solution, and then 1.5 ml was transferred to a square cuvette for DLS measurements and 1 ml was transferred to a Malvern Clear Zeta Potential cell for LDV measurements. Most solutions were made at a concentration of 25 μg/ml; however, sometimes it was necessary, especially with the Al_2O_3, SiO_2, and TiO_2 particles and all CNT, to adjust the concentration higher, such as the 50 μg/ml concentrations, for the device to acquire enough counts per second (Table 1). Solution pH for zeta potential measurements was measured with an IQ Scientific Instruments IQ150 pH meter.

Dispersion Technology Software for Malvern Zetasizer Nano-ZS. The Malvern Zetasizer Nano-ZS uses the Dispersion Technology Software (DTS) (V4.20) for data collection and analysis. The software collects and interprets data for the particle size, zeta potential, and molecular weight measurement functions of the device. For the particle sizing in solution (DLS), the software gives multiple aspects and interpretations of the data collected for the sample such as intensity, volume, and number distribution graphs as well as statistical analysis for each. The mean particle diameter is calculated by the software from the particle distributions measured, and the polydispersity index (PdI) given is a measure of the size ranges present in the solution (Malvern, Instruments Ltd., 2005).

The "raw" intensity data obtained from DLS does bias toward large particles due to their scattering thousands of times more light than smaller particles do. This bias is accounted for by the DTS software by entering the refractive index of the material and absorbance value. From this information, the software adjusts the distribution, either by volume or by number, to give a more realistic relative distribution. It uses the intensity, volume, and number distribution in calculating average size, PdI, and relative %. The PdI scale ranges from 0 to 1, with 0 being monodisperse and 1 being polydisperse. The software calculates the PdI value from the G1 correlation function and from parameters defined in the ISO standard document 13321:1996 E. As for zeta potential measurements, the data are given as either a zeta potential graph or an electrophoretic mobility graph. For all zeta potential measurements made, the Smoluchowski approximation was used since the particles were dispersed in polar solvents.

Cell culture. The mouse keratinocyte cell line, HEL-30, was generously received from the Environmental Health Effects Lab/Naval Health Research Lab, WPAFB, OH. The cells were cultured in flasks with a 1:1 mixture of DMEM/Nutrient F-12 Ham (Ham's F-12) supplemented with 10% HI-FBS and 1% pen/strep and incubated at 37°C in a humidified incubator with 5% CO_2. For nanoparticles exposure protocols, the media that corresponded to the DLS studies was used.

Cell morphology and nanoparticle uptake analysis using CytoViva ultra resolution imaging system. Dual-chamber culture slides were seeded with HEL-30 cells at a concentration of 75,000 cells/ml with 1 ml DMEM/F-12 media, supplemented with 10% HI-FBS and 1% pen/strep, per chamber. Growth media was removed after 24 h incubation, and cells were dosed with various solutions of nanomaterials. After 24 h from dosing, cells were rinsed three times with 1 × phosphate-buffered saline (PBS) solution and were fixed in ice-cold methanol. Samples were evaluated on glass slides with coverslips using the × 60 oil lens and were imaged with an Olympus IX71 Microscope platform coupled to the CytoViva 150 Ultra Resolution Imaging (URI) System, as described in our study by Skebo *et al.* (2007). A QImaging Retiga 4000R and QCapture Pro Imaging Software 6.0 were used to capture and store images.

Cytotoxicity assay. HEL-30 cells were seeded at 15,000 cells per well (75,000 cells/ml with 200 μl per well) and grown in DMEM/F-12 media, supplemented with 10% FBS and 1% pen/strep, until 80% confluent in a 96-well plate, and then specified concentrations of various nanomaterials were added into the wells with different types of media, which corresponded to the DLS studies. The cultures were further incubated for 24 h, dosing solutions aspirated, samples were washed three times with 1 × PBS, 100 μl DMEM/F-12 media with 1% pen/strep was added to each well, and cell proliferation was assessed by adding 20 μl of the CellTiter 96 AQueous One Solution from Promega (Madison, WI) and incubating for 1 h at 37°C. Plates were then read on a Molecular Devices SpectraMax 190 spectrophotometer with Softmax Pro 3.1 software for sample absorbance at a wavelength of 490 nm. The relative cell viability (%) of nanomaterial-dosed wells related to control wells without nanoparticles was calculated by [A]test/[A]control × 100. Where [A]test is the absorbance of the

test sample and [A]control is the absorbance of control sample. Each experiment was done in triplicate, and the data are represented as the mean ± SD.

Postsonication characteristics of PS-Ag 25–30 nm and HC-Ag 25 nm timepoint study. Dilutions of the Ag 25–30 nm and Ag 25 nm were made in sterile deionized water and DMEM/F-12 cell culture media (no serum, 1% pen/strep) at 25 μg/ml and then sonicated for 0, 10, 30, and 60 s at 100% output, which was 35 W delivered to the solution, using a Cole-Parmer 4710 Ultrasonic Homogenizer (probe sonicator).

Cu 40, 60, and 80 nm stock solution timepoint study. Cu 40, 60, and 80 nm nanoparticles were weighed out and suspended in sterile deionized water at a concentration of 1 mg/ml. The solutions were initially sonicated (day 0) for 30 s at 35 W to produce a homogeneous solution and then measurements for particle size and zeta potential were made at intervals over a 1-month period. Between measurements, stock solutions were stored at 4°C, and prior to each measurement, the stock solutions were removed from the refrigerator, warmed to room temperature, vortexed, and then diluted to 25 μg/ml. This procedure was done to mimic the process which stock solutions for *in vitro* toxicology studies complete while in use. The samples were then placed in a zeta potential cell for DLS and LDV measurements.

RESULTS

TEM of Nanoparticles for Primary Size Determination

TEM was used to obtain essential information on primary nanoparticle sizes and morphologies (Figs. 1A–F). All the nanoparticles examined by TEM show similarities in their spherical morphologies and sizes to the manufacturer-specified sizes. Although most of the mean nanoparticle sizes were in agreement with the specified size, there was a great amount of polydispersity in the Al_2O_3 and Al samples, as previously shown by Wagner *et al*. (2007), as well as with the Cu and TiO_2 nanoparticles (Fig. 1). The Al_2O_3 40 nm nanoparticles had a larger mean size than expected of 64.3 nm, and the Al 50 nm nanoparticles had a smaller mean size of 34.7 nm. Additionally, the Cu 60 nm formed compact aggregates, making it difficult to determine individual particle size; however, a rough estimate of mean size was 80 nm. The mean values obtained for primary nanoparticle size serve not only to confirm the manufacturer's size specification but also provide an overall assessment of polydispersity.

In Figure 2, a comparison is given of HC-Ag 15 nm particles dispersed in DI H_2O, RPMI-1640 media, and RPMI-1640 media with 20% serum which have been dried onto the formvar/carbon-coated grid to demonstrate similar conditions for DLS readings. Particles appear to be very loosely agglomerated in Figure 2A, whereas in Figures 2B and 2C, agglomeration increased moderately.

DLS and LDV Particle Characterization in Solution

Since the TEM images and measurements were acquired under high vacuum conditions that require a dry sample,

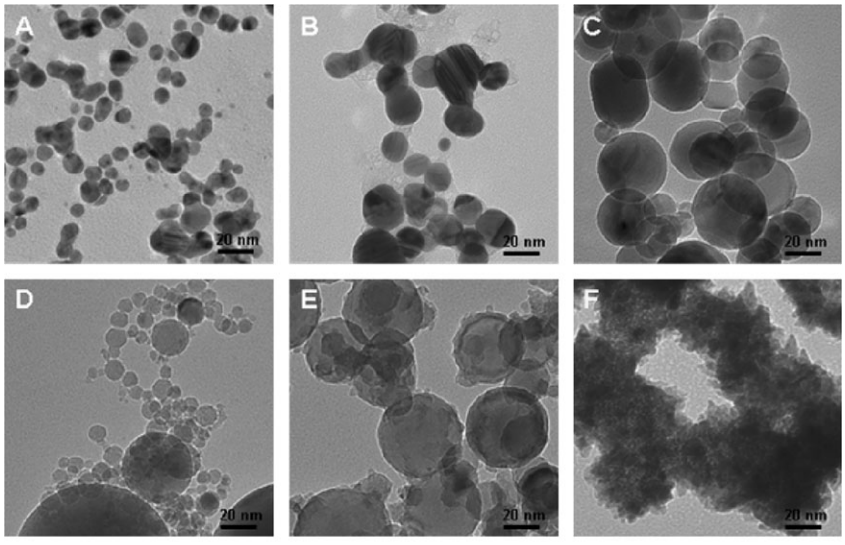

	PS-Ag 10nm	HC-Ag 15nm	TiO_2 39nm	Al_2O_3 40nm	Al 50nm	Cu 60nm*
Mean	9.5 nm	13.3 nm	44.7 nm	64.3 nm	34.7 nm	79.7 nm
S.D.	4.3 nm	7.0 nm	13.0 nm	21.5 nm	17.3 nm	21.3 nm

FIG. 1. Size distributions of various nanoparticles examined with TEM and associated table. Nanoparticle suspensions were dried on formvar/carbon film–coated Cu grids, as described in Materials and Methods section. All images were taken at × 100,000 magnification and 100 kV. A total of 100 particles were measured per sample in TEM for each distribution. Distribution mean and SD presented in associated table. *Due to the aggregation of Cu 60 nm, most individual particle sizes were averaged for distribution data. (A) PS-Ag 10 nm. (B) HC-Ag 15 nm. (C) TiO_2 39 nm. (D) Al_2O_3 40 nm. (E) Al 50 nm. (F) Cu 60 nm.

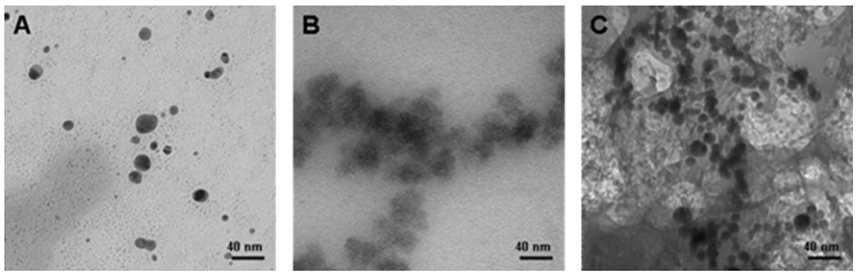

FIG. 2. Comparison TEM images of PS-Ag 10 nm after dispersion in various solvents. PS-Ag 10 nm nanoparticle suspensions were dried on formvar/carbon film–coated Cu grids, as described in Materials and Methods section. All images were taken at × 100,000 magnification and 100 kV. (A) PS-Ag 10 nm in DI H_2O. (B) PS-Ag 10 nm in RPMI-1640 media. (C) PS-Ag 10 nm in RPMI-1640 media with 20% serum added.

further complimentary experiments were performed to obtain size and charge characterization in aqueous or physiological solutions using DLS and LDV. The DLS results for particle size in solution for the Al_2O_3 and Al nanoparticles are presented in Table 2. All the Al-based particles tended to form agglomerates of similar size when dispersed in either water or cell culture media. The Al_2O_3 30 and 40 nm particles ranged from 210 and 237 nm in water to 223 and 251 nm in F-12K media with serum. Both agglomerated highly in F-12K media without serum with values reaching 1430 nm for Al_2O_3 30 nm, and 1050 nm for Al_2O_3 40 nm. Al 50 nm particles were 253 nm in water, 1170 nm in DMEM/F-12 media, and 395 nm in DMEM/F-12 media with serum. Al 80 and 120 nm particles showed a change in agglomeration size, when comparing dispersion in water to DMEM/F-12 media with serum, from 378 to 355 nm and 342 to 535 nm, respectively. The Al 80 and 120 nm also agglomerated highly in DMEM/F-12 media only with values at 1390 and 1610 nm, respectively. The results from reading the zeta potential of these particles are also presented in Table 2. The Al_2O_3 30 nm having the highest zeta potential at 43.0 mV, next was Al_2O_3 40 nm at 36.2 mV, then Al 50 nm at 34.8 mV, and finally Al 120 nm and Al 80 nm were similar at 28.4 mV and 26.5 mV, respectively.

As seen in Table 3, the Ag-based particles exhibited a similar pattern by agglomerating at nearly the same size when dispersed in either water or media with serum. PS-Ag 80 nm was the only exception to this trend, showing an increase from 250 nm in water to 1230 nm in RPMI-1640 media with serum. Again, higher agglomeration sizes were seen in the media without serum samples; however, the Ag 80 nm and PS-Ag 80 nm did not follow this trend. The Ag 80 nm particles in media without serum showed approximately a 50% decrease in agglomeration when compared to the water sample. The PS-Ag 80 nm sample showed an increasing trend from 250 nm in water to 743 nm in media and finally 1230 nm in media with serum. PdI values for each sample varied slightly; however, the Ag 80 nm, PS-Ag 10 nm, and PS-Ag 80 nm changed increased more significantly. The LDV results are included in Table 3, where most particles had zeta potentials around 20–25 mV, with the PS-Ag 10 nm having the highest at 58.4 mV.

Cu 40, 60, and 80 nm particles were observed after dispersion in water, media, and media with serum (Table 4). Cu 60 and 80 nm exhibited increased agglomeration in media and decreased agglomeration in media with serum when compared with water. Agglomeration sizes in water were 423 and 372 nm, while in media with serum, sizes were 379 and 410 nm for Cu 60 nm and Cu 80 nm, respectively. Cu 40 nm

TABLE 2
DLS and LDV Data for Various Al_2O_3 and Al Nanoparticles

	DLS		LDV		
Particle	Average diameter (nm)	PdI	Zeta potential ζ (mV)	Electrophoretic mobility U (μmcm/(Vs))	pH
Al_2O_3 30 nm					
DI H_2O	210	0.125	43.0	3.36	7.0
RPMI-1640 media	1430	0.373	***	***	7.2
RPMI-1640 media wt/ 20% serum	223	0.23	***	***	7.5
Al_2O_3 40 nm					
DI H_2O	237	0.145	36.2	2.84	7.0
RPMI-1640 media	1050	0.232	***	***	7.2
RPMI-1640 media wt/ 20% serum	251	0.252	***	***	7.5
Al 50 nm					
DI H_2O	253	0.224	34.8	2.73	7.0
F-12K media	1170	0.247	***	***	7.2
F-12K media with 20% serum	395	0.393	***	***	7.5
Al 80 nm					
DI H_2O	378	0.422	26.5	2.08	7.0
F-12K media	1390	0.268	***	***	7.2
F-12K media with 20% serum	355	0.398	***	***	7.5
Al 120 nm					
DI H_2O	342	0.341	28.4	2.23	7.0
F-12K media	1610	0.25	***	***	7.2
F-12K media with 20% serum	535	0.821	***	***	7.5

Note. Particles were dispersed in DI H_2O, RPMI-1640 media with and without serum or F-12K media with and without serum. Mixing was done via bath sonication and vortexing, and samples were measured at 25 or 50 μg/ml.

TABLE 3
DLS and LDV Data for Various Ag Nanoparticles

Particle	DLS		LDV		
	Average diameter (nm)	PdI	Zeta potential ζ (mV)	Electrophoretic mobility U (μmcm/(Vs))	pH
HC-Ag 15 nm					
DI H_2O	148	0.398	− 23.4	− 1.84	7.0
RPMI-1640 media	396	0.241	***	***	***
RPMI-1640 media wt/ 20% serum	153	0.257	***	***	***
HC-Ag 25 nm					
DI H_2O	208	0.44	− 20.6	− 1.62	7.0
RPMI-1640 media	499	0.374	***	***	***
RPMI-1640 media wt/ 20% serum	182	0.356	***	***	***
Ag 80 nm					
DI H_2O	1810	1	− 20.4	− 1.6	7.0
RPMI-1640 media	977	0.835	***	***	***
RPMI-1640 media wt/ 20% serum	1640	0.9	***	***	***
PS-Ag 10 nm					
DI H_2O	72.8	0.179	− 58.4	− 4.57	7.0
RPMI-1640 media	413	0.316	***	***	***
RPMI-1640 media wt/ 20% serum	49.4	0.541	***	***	***
PS-Ag 25–30 nm					
DI H_2O	128	0.235	− 25.9	− 2.03	7.0
RPMI-1640 media	261	0.301	***	***	***
RPMI-1640 media wt/ 20% serum	118	0.192	***	***	***
PS-Ag 80 nm					
DI H_2O	250	0.398	− 20.3	− 1.59	7.0
RPMI-1640 media	743	0.414	***	***	***
RPMI-1640 media wt/ 20% serum	1230	0.893	***	***	***

Note. Ag, HC-Ag, and PS-Ag particles were dispersed in DI H_2O and RPMI-1640 media with and without serum. Mixing was done via bath sonication and vortexing, and samples were measured at 25 μg/ml.

TABLE 4
DLS and LDV Data for Various Cu Nanoparticles

Particle	DLS		LDV		
	Average diameter (nm)	PdI	Zeta potential ζ (mV)	Electrophoretic mobility U (μmcm/(Vs))	pH
Cu 40 nm					
DI H_2O	1120	0.374	− 4.75	− 0.373	7.0
RPMI-1640 media	1110	0.399	***	***	***
RPMI-1640 media wt/ 20% serum	340	1	***	***	***
Cu 60 nm					
DI H_2O	423	0.237	− 11.6	− 0.906	7.0
RPMI-1640 media	532	0.242	***	***	***
RPMI-1640 media wt/ 20% serum	379	0.504	***	***	***
Cu 80 nm					
DI H_2O	372	0.219	− 13.1	− 1.02	7.0
RPMI-1640 media	510	0.224	***	***	***
RPMI-1640 media wt/ 20% serum	410	0.577	***	***	***

Note. Particles were dispersed in DI H_2O and RPMI-1640 media with and without serum. Mixing was done via bath sonication and vortexing, and samples were measured at 25 μg/ml.

agglomerated highly in water and media without serum with sizes of 1120 and 1110 nm, while in media serum, agglomeration sizes decreased to 340 nm. For zeta potential readings, Cu 40 nm was lowest with − 4.75 mV, Cu 60 nm was next with − 11.6 mV, and highest was Cu 80 nm with − 13.1 mV (Table 4).

Two different studies were completed with TiO_2 particles, one with varying crystalline structures and one with varying sizes. The TiO_2 crystalline structures evaluated were TiO_2 39 nm (100% anatase), TiO_2 39 nm (61% rutile, 39% anatase), TiO_2 39 nm (40% rutile, 60% anatase), and TiO_2 40 nm amorphous (Table 5). The amorphous TiO_2 maintained high agglomeration values for all three solvents, with 1300 nm in water, 2040 nm in media, and 1890 nm in media with serum. The other TiO_2 particles were below 800 nm in water, and only the TiO_2 61% rutile showed a significant decrease after dispersion in media with serum, dropping to 257 nm from 2510 nm in media only. TiO_2 61% rutile also had the largest zeta potential of the group at 17.7 mV.

The sizes of TiO_2 evaluated were 5, 10, 16, 50, and 100 nm (Table 6). Even with a wide range of primary particle sizes, all particles tested, except TiO_2 10 nm, exhibited high agglomeration in all three solvents with sizes above 1500 nm in water, above 1430 nm in media, and above 1720 nm in media with serum. TiO_2 10 nm was measured below these ranges only when dispersed in water, with an average diameter of 216 nm. Zeta potentials varied widely for these samples, with TiO_2 10 nm having the largest at 15 mV.

The SiO_2 particles and SiO_2-coated fluorophores were the only groups of particles tested which dispersed at, or very closely to, their primary particle size. As seen in Table 7, the SiO_2 35, 51, and 110 nm particles measured 28.9, 52.9, and 121 nm when dispersed in DI H_2O and 39, 51.9, and 119 nm when in cell dosing media. The SiO_2 420 nm particle was not as close to the primary size, measuring 704 nm in water and 982 nm in dosing media. All zeta potential values were larger than − 23 mV and SiO_2 420 nm having the largest value of the group at − 39 mV.

The SiO_2-FITC and SiO_2-RB were approximated to have a 73-nm diameter by the supplier. The DLS results in Table 7 shows agglomeration of the SiO_2-FITC particles to 145 nm in water, with this value decreasing to 53.5 nm in media. The SiO_2-RB particles measured 74.1 nm in water and 51.8 nm in media. LDV results for both are in Table 7, with each particle measuring around − 25 mV.

TABLE 5
DLS and LDV Data for TiO_2 Nanoparticles with Various Crystalline Structures

	DLS		LDV		
Particle	Average diameter (nm)	PdI	Zeta potential ζ (mV)	Electrophoretic mobility U (μmcm/(Vs))	pH
TiO_2 39 nm, 100% anatase					
DI H_2O	486	0.737	− 4.95	− 0.388	7.0
DMEM/F-12 media	1760	0.506	***	***	7.5
DMEM/F-12 media with serum	1300	0.549	***	***	7.5
TiO_2 39 nm, 60% anatase, 40% rutile					
DI H_2O	519	0.661	13	1.02	7.0
DMEM/F-12 media	2030	0.743	***	***	7.5
DMEM/F-12 media with serum	1780	0.743	***	***	7.5
TiO_2 39 nm, 39% anatase, 61% rutile					
DI H_2O	796	0.654	17.7	1.39	7.0
DMEM/F-12 media	2510	0.408	***	***	7.5
DMEM/F-12 media with serum	257	0.362	***	***	7.5
TiO_2 40 nm amorphous					
DI H_2O	1300	0.282	− 12.1	− 0.95	7.0
DMEM/F-12 media	2040	0.349	***	***	7.5
DMEM/F-12 media with serum	1890	0.435	***	***	7.5

Note. Particles were all 39 or 40 nm and were dispersed in DI H_2O and Ham's F-12 media. Mixing was done via bath sonication and vortexing, and all samples were measured at 50 μg/ml.

TABLE 6
DLS and LDV Data for TiO_2 Nanoparticles with Various Sizes

	DLS		LDV		
Particle	Average diameter (nm)	PdI	Zeta potential ζ (mV)	Electrophoretic mobility U (μmcm/(Vs))	pH
TiO_2 5 nm					
DI H_2O	2710	0.336	− 3.75	− 0.294	7.0
DMEM/F-12 media	1430	0.367	− 6.01	− 0.471	7.2
DMEM/F-12 media wt/ 10% serum	2170	0.196	***	***	7.2
TiO_2 10 nm					
DI H_2O	216	0.439	15	1.18	7.0
DMEM/F-12 media	1790	0.264	***	***	7.2
DMEM/F-12 media wt/ 10% serum	2570	0.193	***	***	7.2
TiO_2 16 nm					
DI H_2O	1500	0.244	7.09	0.556	7.0
DMEM/F-12 media	1810	0.225	***	***	7.2
DMEM/F-12 media wt/ 10% serum	1720	0.259	***	***	7.2
TiO_2 50 nm					
DI H_2O	1610	0.233	1.77	0.139	7.0
DMEM/F-12 media	2300	0.314	***	***	7.2
DMEM/F-12 media wt/ 10% serum	2280	0.287	***	***	7.2
TiO_2 100 nm					
DI H_2O	1510	0.259	4.07	0.319	7.0
DMEM/F-12 media	2500	0.506	***	***	7.2
DMEM/F-12 media wt/ 10% serum	2480	0.614	***	***	7.2

Note. Particles were dispersed in DI H_2O and DMEM/F-12 media with and without serum added. Mixing was done via bath sonication and vortexing, and all samples were measured at 50 μg/ml.

In Table 8, DLS and LDV data for three types of CNT and a spherical CB sample are reported. To see if data could be obtained for high aspect ratio materials, measurements were collected in water for SWNT, MWNT-COOH, and CNT with mean size values at 900, 825, and 821 nm along with very high PdI readings. The CB sample was analyzed in DMEM/F-12 cell culture media with and without serum. Agglomeration sizes ranged from 396 to 2190 nm depending upon the solvent used. SWNT had the largest zeta potential of the group at 50.2 mV.

X-Ray Photoelectron Spectroscopy

XPS was used to detect the elements present within approximately the outermost 1–3 nm of the nanoparticle surface. For the PS-Ag 10 nm sample, an abundance of C-H groups were present along with C=O, O-C-O, and C-O groups, which are characteristic of polysaccharides as shown by a typical XPS measurement in Figure 3. The elemental Ag signal from the Ag-based nanoparticles was completely masked due to the thickness of the polysaccharide coating. The low levels of Na and S detected are probably due to the presence of a dispersant (DAXAD), which is a sodium salt of a high molecular weight naphthalene sulfonate formaldehyde condensate used as a stabilizing agent (Sondi *et al*., 2003).

Cell Morphology

The morphology of the HEL-30 control cells, grown without and with serum present in the RPMI-1640 media, showed little difference (Figs. 4A and 4B). The only noticeable difference was a slightly higher confluency, or density, of the cells grown in media with serum. Cells dosed with HC-Ag 15 nm without serum retracted into a smaller spherical shape with numerous particles coating the surface and exhibited decreased confluency from control, which can be seen in Figure 4C. With serum present, the HC-Ag 15 nm particle–dosed cells exhibited reduced cell-to-cell extensions and smaller cytoplasms (Fig. 4D). Cell confluency decreased minimally and was similar in confluency to the control without serum. The Al_2O_3 30 nm–dosed cells without serum seem to have near-normal

TABLE 7
DLS Data for SiO_2 and SiO_2-Coated Fluorophore Nanoparticles

	DLS		LDV		
Particle	Average diameter (nm)	PdI	Zeta potential ζ (mV)	Electrophoretic mobility U (μmcm/(Vs))	pH
SiO_2 35 nm					
DI H_2O	28.9	0.093	− 23.1	− 1.81	7.0
DMEM/F-12 media	39	0.116	***	***	7.2
SiO_2 51 nm					
DI H_2O	52.9	0.07	− 30.1	− 2.36	7.0
DMEM/F-12 media	51.9	0.069	***	***	7.2
SiO_2 110 nm					
DI H_2O	121	0.007	− 33.1	− 2.59	7.0
DMEM/F-12 media	119	0.018	***	***	7.2
SiO_2 420 nm					
DI H_2O	704	0.235	− 39	− 3.06	7.0
DMEM/F-12 media	982	0.21	***	***	7.2
SiO_2-FITC ~73 nm					
DI H_2O	145	0.245	− 25.2	− 2	7.0
F-12K media	53.5	1	***	***	7.5
SiO_2-RB ~73 nm					
DI H_2O	74.1	0.213	− 27.4	− 2.15	7.0
F-12K media	51.8	0.587	***	***	7.5

Note. Particles were dispersed in DI H_2O and DMEM/F-12 media without serum. Mixing was done via vortexing, and all samples were measured at 50 μg/ml.

morphology, but the particles appear to bind to the surface of the cells making it difficult to distinguish individual cells (Fig. 4E). In the Al_2O_3 30 nm–dosed cells with serum, cell morphology remains normal while confluency is decreased slightly when compared to control with serum. The particles do not appear to adhere to surface of cells as readily when compared to the sample dosed without serum (Fig. 4F).

TABLE 8
DLS and LDV Data for CNT and CB

	DLS		LDV	
Particle	Average diameter (nm)	PdI	Zeta potential ζ (mV)	Electrophoretic mobility U (μmcm/(Vs))
SWNT				
DI H_2O	900	0.816	50.2	3.94
MWNT-COOH				
DI H_2O	825	0.799	− 15.7	− 1.23
CNT-1				
DI H_2O	821	0.562	− 13.6	− 1.07
CB				
DI H_2O	396	0.207	− 1.56	− 0.123
DMEM-F-12	2190	0.648	***	***

Note. Mixing was done via bath sonication and vortexing, and samples were measured at 25 or 50 μg/ml.

Cell Viability

MTS assays, 3-(4,5-dimethylthiazol-2-yl)-5-(3-carboxymethoxyphenyl)-2-(4-sulfophenyl)-2H-tetrazolium combined with phenazine ethosulfate, were conducted to assess cellular mitochondrial function, which was correlated to viability of the HEL-30 cells. Particles were chosen for this study from the DLS data by comparing their size when dispersed in media and their size in media with serum. If the DLS data showed a significant difference in average agglomerate size from media to media with serum, then the particle was deemed necessary to test for *in vitro* toxicity differences due to possible serum influence. Cells were dosed with solutions identical in composition and concentration to samples measured by DLS.

For samples dosed in RPMI-1640 media, cell proliferation data are presented in Figure 5. Al_2O_3 particles showed no significant difference between dosing with or without serum; however, both the Al_2O_3 30 nm samples showed a slight increase in proliferation over the control samples. The Al_2O_3 40 nm samples exhibited no significant difference from control samples. Proliferation decreased to 30% for the HC-Ag 15 nm and 20% for the PS-Ag 10 nm when dosed in RPMI-1640 media without serum. With serum present, both the HC-Ag 15 nm and PS-Ag 10 nm samples returned to near-control proliferation values. The Cu 60 nm samples' proliferation decreased to 45% when exposed to the cells in media without serum and slightly increased to 70% when serum was added.

MTS data from samples dosed to the cells in F-12K media are presented in Figure 6. The Al 50 nm and Al 80 nm samples, for the majority, did not exhibit any toxicity except for the Al 80 nm sample dosed with serum, which decreased a small amount to 85%. Both the Al 120 nm samples showed decreased proliferation to 70–75%.

In Figure 7, the MTS data for the TiO_2 39 nm and CB samples exposed in DMEM/F-12K are shown. The TiO_2 39 nm (39% anatase, 61% rutile) decreased proliferation to 80% in both the media without serum and media with serum samples. The CB demonstrated 55% proliferation, when compared to control, for the media without serum sample, and 60% proliferation for the media with serum sample.

Postsonication Characterization of Nanoparticle Solutions

Preliminary studies to test the effects of probe sonication on nanoparticle characteristics in stock (water) and dosing (media) solutions were completed. In Figures 8A and 8B, a sample of HC-Ag 25 nm dispersed in DI H_2O was subjected to probe sonication at approximately 35 W with increasing duration from 0 to 60 s. Figure 8A shows the zeta potential change for PS-Ag 25–30 nm with increasing sonication time, while Figure 8B shows the change in zeta potential of the HC-Ag 25 nm particles for the same sonication times. As seen in the graphs, the zeta potential for the PS-Ag 25–30 nm sample decreased in magnitude from − 31 mV with no sonication to − 16 mV at 10 s sonication and then increased in magnitude to − 23 mV after

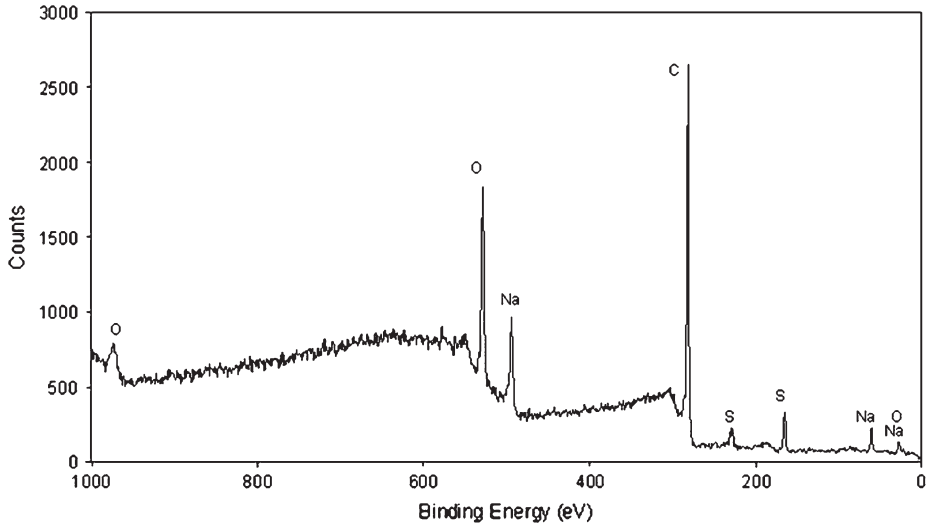

PS-Ag 10nm	C			O	Ag	Na	N	S
	C=O,O-C-O	C-O	C-H, C					
- 1	1.2	3.8	62.6	20.0	0.2	9.0	0.5	2.7
- 2	1.2	4.3	61.8	20.2	< 0.1	8.8	0.7	2.9

FIG. 3. XPS of PS-Ag 10 nm and associated table showing the approximate atomic % elemental surface composition. Graph shows characteristic peaks detected and with labels of possible element for peak. Notice detection of Na and S. Table shows relative atomic % for each element.

60 s sonication. The zeta potential for this sample changed from − 16 mV with no sonication to − 14 mV after 60 s sonication. In Figures 8C and 8D, the same sonication technique was applied to the PS-Ag 25–30 nm and the HC-Ag 25 nm samples dispersed in DI H_2O and RPMI-1640 media with 20% serum. For the PS-Ag 25–30 nm sample, the mean diameter changed from 110 to 70 nm in water and from 290 to 200 nm in media after 60 s sonication. The lowest mean diameter reached for the PS-Ag 25–30 nm in water was at 60 s, while the same sample in media was lowest after 10 s. The average size in media increased after the 10-s timepoint. The HC-Ag 25 nm sample in water followed a similar pattern to the PS-Ag 25–30 nm sample in water, changing from an average agglomerate size of 150–85 nm after 60 s sonication. The HC-Ag 25 nm in media with serum increased in mean particle size over the nonsonicated sample at all sonication times, increasing from 390 to 500 nm after 60 s sonication.

Timepoint Study of Nanoparticle Stock Solution

Analysis of the stock solutions of particles used for toxicity evaluations is necessary to understand the length of time a particle in solution will retain its properties which it possesses when it is initially dispersed. Cu nanoparticles were analyzed in this study due to their highly oxidative nature and observed morphological changes after time in solution. Particles were observed under TEM to change from a more solid, spherical particle (Figs. 9A–C) to a smaller, spherical center particle with crystalline spikes emanating from the surface after 1 month in solution (Figs. 9D–F). All the Cu nanoparticles exhibited this phenomenon.

Figure 10A shows the change in mean particle size from initial dispersion into water with 30 s sonication to 34 days after dispersion. Initially, all particles were approximately 400 nm when dispersed into DI H_2O. After 34 days, Cu 40 nm increased to 1150 nm, Cu 60 nm increased to 820 nm, and Cu 80 increased to 1510 nm. Figure 10B shows the zeta potential change over the 34-day period, and the same sample used for the particle size measurements were used to the measure zeta potential. As seen in Figure 10B, all three samples were at, or above, 30 mV initially, but within 7-days after dispersion, there was a significant decline in zeta potential. Following this initial decrease, the zeta potential for all three Cu nanoparticles increased and for Cu 40 and 80 nm this value stabilized near 30 mV. In contrast, the zeta potential for Cu 60 continued to decrease and the final reading was practically 0 mV 34 days after dispersion.

DISCUSSION

In this study, various nanoparticles were examined in physiologically relevant solutions to better understand changes to their characteristics when in an aqueous solution prior to toxicity studies. TEM was used to determine the primary size

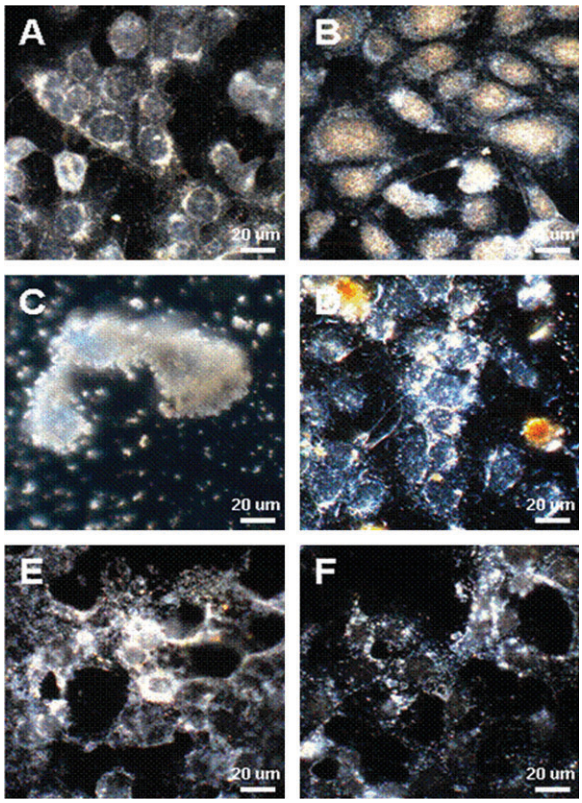

FIG. 4. Cell morphology study of HEL-30 cells using CytoViva. Light microscopy images captured using CytoViva URI system equipped with QImaging Retiga 4000R camera using procedure described in Materials and Methods section. All pictures obtained at × 96 magnification. (A) Control cells exposed to RPMI-1640 media without serum. (B) Control cells exposed to RPMI-1640 media with serum. (C) Cells dosed with HC-Ag 15 nm particles at 25 μg/ml without serum present. (D) Cell dosed with HC-Ag 15 nm particles at 25 μg/ml with serum present. (E) Cells dosed with Al_2O_3 30 nm particles without serum present. (F) Cells dosed with Al_2O_3 30 nm particles with serum present. Table shows corresponding MTS data for comparison to morphology images.

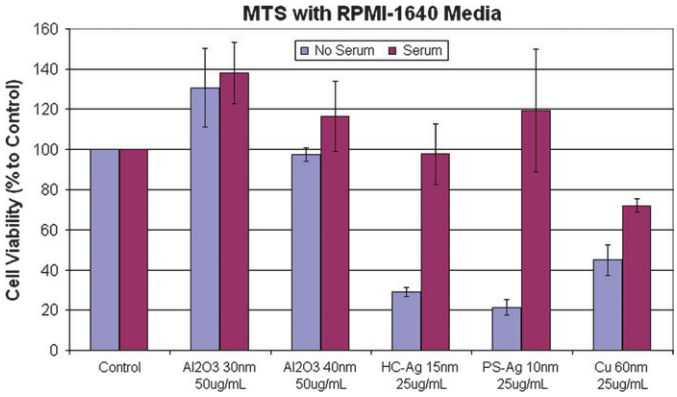

FIG. 5. Effect of nanomaterials dispersed in RPMI-1640 media and RPMI-1640 media with serum on mitochondrial function in HEL-30 Cells. MTS assay was performed after 24-h exposure as described in Materials and Methods section. The exposure was conducted with or without serum with their respective controls. Each data set mean value is a composite of three independent experiments with SD shown.

and morphology of nanoparticles in dry form. Due to the nanoparticle suspensions being dried for imaging under the high vacuum conditions in the TEM, it cannot provide an accurate representation of the relative dispersion of the nanoparticles in solution prior to exposure. For this reason, DLS was utilized for its ability to analyze particle dimension in solution. By comparing the primary particle size obtained with TEM to the average size in water with DLS, several general trends were revealed.

The media type and serum concentrations for particle dispersion and measurement were chosen to specifically coincide with current *in vitro* experimentation. Hence, it was not deemed necessary to try every possible combination of various cell culture media, serums, and particles. One trend discovered from these measurements was an apparent reduction of agglomeration in cell culture media with serum possibly because the proteins in the serum seem to mitigate agglomeration. The Al_2O_3, Al, Ag, and Cu particles displayed this phenomenon more significantly than the others tested. As seen by the zeta measurements, only a few particles had zeta potential values higher than the + 30 mV/− 30 mV line for stable dispersion (Malvern, Instruments Ltd., 2005; Müller, 1996). Having these higher values allowed them to disperse at smaller sizes, increasing the exposed surface area and possibly allowing for more interaction with serum proteins. The Al_2O_3, Al, and Ag particles in particular had larger than ± 20 mV zeta potentials, suggesting that there could be electrostatic attraction to proteins when in media with serum. This interaction could explain the reduced agglomerate sizes observed. This interaction of particles with serum proteins will need to be investigated further to identify the interacting proteins, to

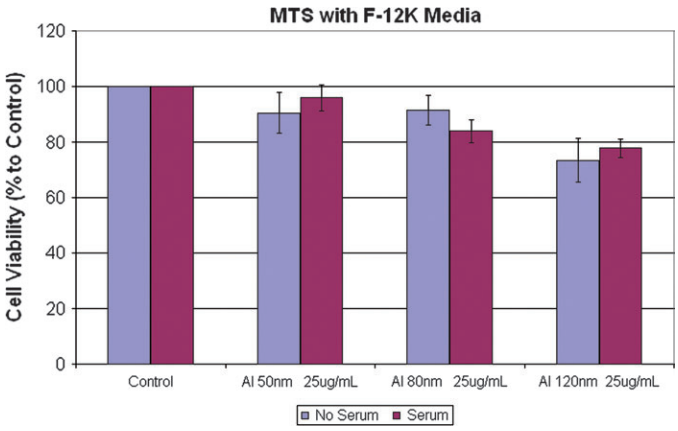

FIG. 6. Effect of nanomaterials dispersed in F-12K media and F-12K media with serum on mitochondrial function in HEL-30 Cells. MTS assay was performed after 24-h exposure as described in Materials and Methods section. The exposure was conducted with or without serum with their respective controls. Each data set mean value is a composite of three independent experiments with SD shown.

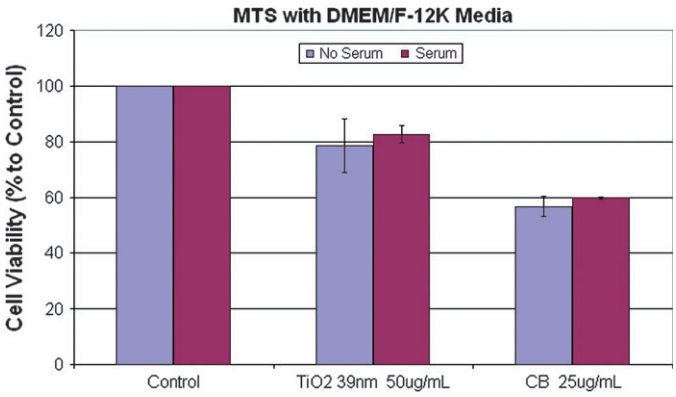

FIG. 7. Effect of nanomaterials dispersed in DMEM/F-12 media and DMEM/F-12 media with serum on mitochondrial function in HEL-30 cells. MTS assay was performed after 24-h exposure as described in Materials and Methods section. The exposure was conducted with or without serum with their respective controls. Each data set mean value is a composite of three independent experiments with SD shown.

determine the extent of the interaction, the size of the proteins interacting, and if they are used by the cell after interaction.

Al_2O_3 nanoparticles agglomerated in DI H_2O and RPMI-1640 media with serum between three and six times their primary particle sizes as measured in TEM. A similar size change was observed for Al nanoparticles with a three to five times increase in size once introduced into DI H_2O and RPMI-1640 media with serum. Both particles exhibited at least a 13-fold increase over primary size when dispersed into media without serum. As can be seen with the cell viability assays (Figs. 4 and 5), neither of the Al_2O_3 or Al nanoparticles exhibited a significant difference between toxicity when serum was or was not present. In a previous study conducted (Wagner *et al*., 2007), Al nanoparticles showed significantly higher toxicity than the Al_2O_3 nanoparticles when exposed to rat alveolar macrophages. It was concluded that the main cause of toxicity relied more on the chemical composition and surface chemistry rather than on particle size. The Al_2O_3 particles did not appear to be toxic when dosed without serum; therefore, the addition of serum did not have much effect even if surface chemistry changed. The Al nanoparticles exhibited a slight increase in toxicity with increasing particle size; however, with serum present, the toxicity was not affected significantly. In this case, the serum proteins may not interact with the particles or change surface chemistry significantly. Although, the images captured with CytoViva in Figure 3E shows that the Al_2O_3 30 nm particles, without serum present, adhere readily to the surface of the cells, they do not affect the overall morphology. In Figure 3F, the Al_2O_3 30 nm particles, with serum present, adhere significantly less to the membrane, suggesting interaction and modification of the nanoparticle and/or differences in cell membrane characteristics.

The HC-Ag, PS-Ag, and uncoated Ag did not demonstrate any remarkable differences in dispersion. There was reduced agglomeration, almost a 50% decrease, observed with PS-Ag in DI H_2O and RPMI-1640 media with serum as compared to the HC-Ag. However, these values are not considered significant since the absolute difference in mean size was only 70–100 nm and that the agglomerates were still four to seven times larger than the primary particle sizes. Both HC-Ag 15 nm and PS-Ag 10 nm particles displayed significant toxicity, reducing viability to 20–30%, when exposed in RPMI-1640 media without serum (Fig. 4). Interestingly, when dosed with serum present, cell proliferation returned to control levels. This indicates a strong interaction between serum proteins and silver nanoparticles. Images from the CytoViva system demonstrate this vast difference in toxicity (Figs. 3C and 3D). The cells exposed to HC-Ag 15 nm without serum were severely decreased in confluency, with the remaining cells showing very round morphologies, typical of cells under stress, and almost completely covered in particles. The cells from HC-Ag 15 nm samples with serum added demonstrate near-normal growth and morphology. One possible explanation for the slightly higher toxicity, when dosed without serum, of the PS-Ag 10 nm compared to the HC-Ag 15 nm is that observations have been made via SEM on fixed mouse germ-line stem cells that higher amounts of PS-Ag particles are taken up by the cell due to this coating (unpublished data, Murdock, R. and Braydich-Stolle, L.). Also, the XPS analysis of the PS-Ag 10 nm particle revealed the presence of another dispersant aid, DAXAD, which has significant levels of Na and S present. The specific effects of this dispersant are unknown at this time; however, it was not known to be present until after the XPS analysis was completed.

Cu 40 nm agglomerated highly in DI H_2O and RPMI-1640 media, achieving sizes 28 times larger than its primary size. This agglomeration decreased after the addition of serum to the media to only nine times primary size. Cu 60 and 80 nm displayed a trend similar to the Al-based and Ag-based particles with aggregates four to seven times larger than primary particle size forming in DI H_2O and RPMI-1640 media with serum. In RPMI-1640 media without serum, Cu 60 nm and Cu 80 nm both increased 7–10 times over primary size. Cu 60 nm decreased cell proliferation to nearly 40% when dosed without serum. After serum was added, viability increased moderately to 70%, indicating some influence from serum proteins. The proteins might be binding to the Cu nanoparticle surface, changing surface chemistry, or by interacting with and reducing the amount of Cu^+ ions in solution. In previous experiments with rat adrenal gland (PC-12) cells, Cu nanoparticles have been seen to cause oxidative stress (unpublished data, Murdock, R.), a likely mechanism for toxicity. Also, manganese nanoparticles have caused dopamine depletion in PC-12 cells due to oxidative stress (Hussain *et al*., 2006).

When the variations in TiO_2 particle crystalline structure were analyzed, it was observed that increasing percentages of rutile structure increased agglomeration sizes in DI H_2O, with the amorphous structure showing the largest agglomeration sizes. On the other hand, this trend was not seen when the particles were dispersed in DMEM/F-12 media with serum.

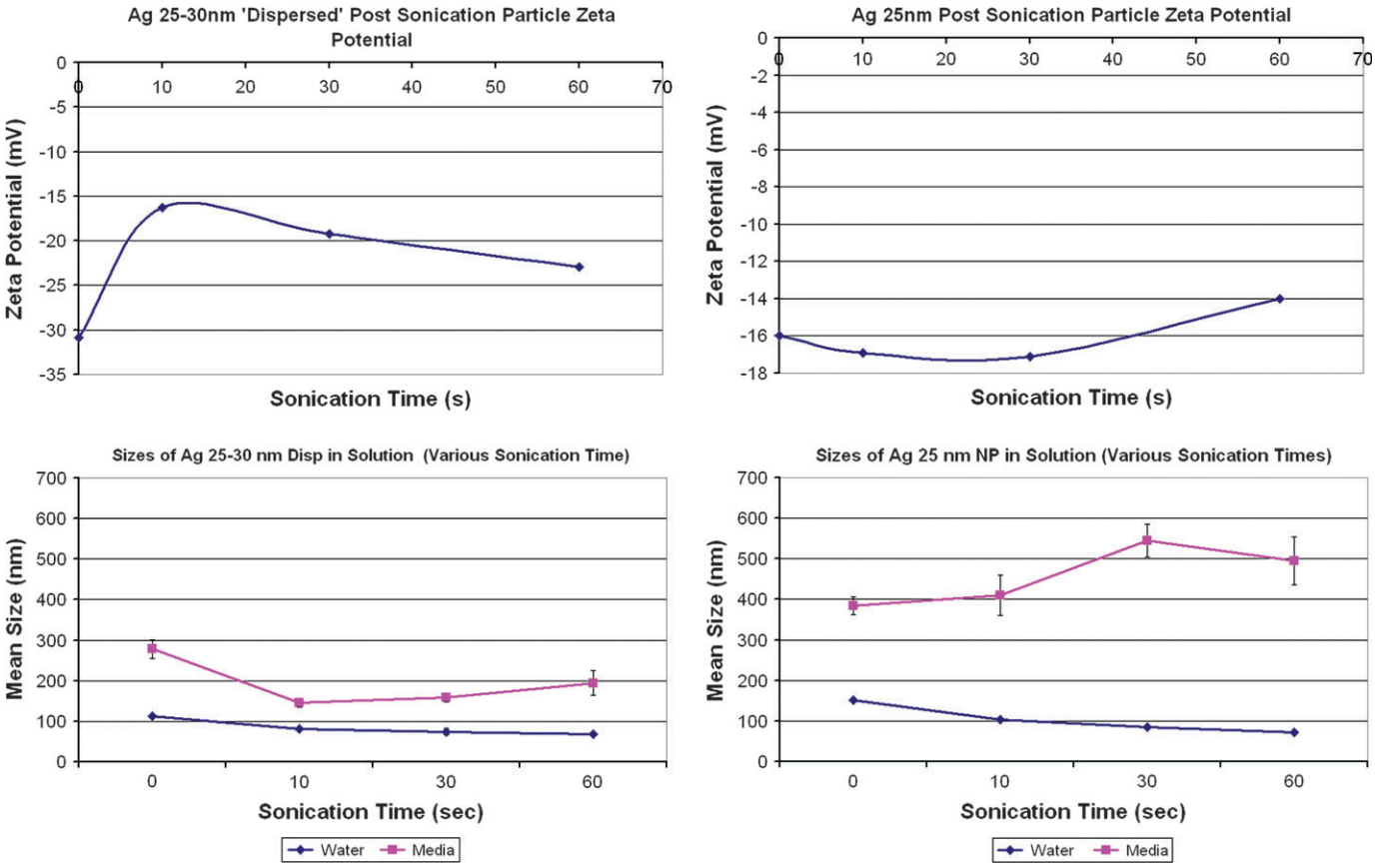

FIG. 8. Effects of increasing sonication times on dispersion of Ag 25 nm and Ag 25–30 nm particles in DI H_2O and cell culture media. (A) Zeta potentials of Ag 25–30 nm in DI H_2O after 0, 10, 30, and 60-s sonication. (B) Zeta potentials of Ag 25 nm in DI H_2O after 0, 10, 30, and 60-s sonication. (C) Comparison of Ag 25–30 nm mean agglomerate sizes in DI H_2O and cell culture media (RPMI-1640, 20% serum) after 0, 10, 30, and 60-s sonication. (D) Comparison of Ag 25 nm mean agglomerate sizes in DI H_2O and cell culture media (RPMI-1640, 20% serum) after 0, 10, 30, and 60-s sonication.

Except for TiO_2 39 nm (39% anatase, 61% rutile), the TiO_2 particles dispersed in media with serum agglomerated to sizes greater than 1 μm. The TiO_2 39 nm (39% anatase, 61% rutile) particle attained agglomerate sizes of ~250 nm when in media with serum, possibly indicating some protein interaction which could be explained by its 17.7-mV zeta potential, the highest of the group. The TiO_2 particle group with increasing particle size was analyzed with only the TiO_2 10 nm exhibiting any significant behavior. The TiO_2 10 nm particle showed mean agglomerate sizes of 216 nm in DI H_2O, the smallest of the group, and also having the largest zeta potential at 15 mV. The TiO_2 39 nm (39% anatase, 61% rutile) particles did not show any difference in toxicity when dosed with or without serum present in the DMEM/F-12 media, with viability around 80% for both.

The only particles observed which dispersed at, or near, their primary particle size were the SiO_2 particles, and this feature did not vary depending on the solvent used. However, the SiO_2 fluorophores were measured multiple times due to some interference from sample fluorescence. The particles were allowed to photobleach at room temperature for 24 h to help reduce fluorescence of the particles before measurement. This significantly reduced the error observed when compared to samples directly taken from the stock solution, diluted, and read immediately. Both samples showed sizes close to the primary particle size when dispersed in water and media. The SiO_2 particles had consistently higher zeta potential values for all sizes which could explain part of the reason for their individual dispersion. However, the microemulsion technique used to manufacture the particles produces a particle with a hydrophilic surface which would significantly decrease the attraction between the individual particles and possibly cause a less toxic *in vitro* response (Gao, 2005; Lee, 2005). These particles were not tested *in vitro* for this communication due to the SiO_2 particles being monodisperse in any solution, as shown by the DLS data, thus being excluded from toxicity assays since no effect on size was seen with presence of serum in cell culture media.

The main goal of studying the CNT was to investigate if this technique was a viable method for analyzing high aspect ratio materials in solution. Since it was observed that the CNT highly agglomerate in DI H_2O, it is difficult to make a judgment about using DLS for carbon nanotube size measurements.

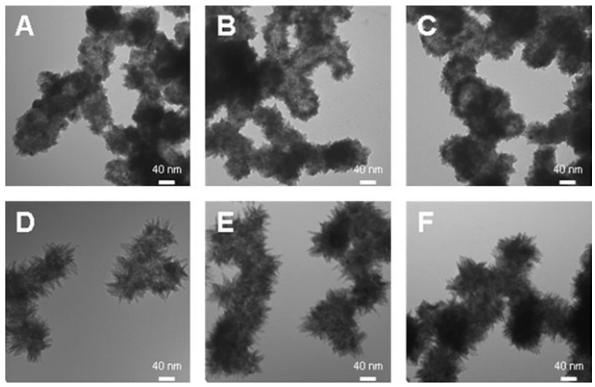

FIG. 9. Comparison TEM images of Cu nanoparticles after 1 day and after 1 month in DI H_2O. Cu nanoparticle suspensions were dried on formvar/carbon film–coated Cu grids, as described in Materials and Methods section. All images taken at × 100,000 magnification and 100 kV. (A) Cu 40 nm after 24 h in solution. (B) Cu 60 nm after 24 h in solution. (C) Cu 80 nm after 24 h in solution. (D) Cu 40 nm after 34 days in solution. (E) Cu 60 nm after 34 days in solution. (F) Cu 80 nm after 34 days in solution.

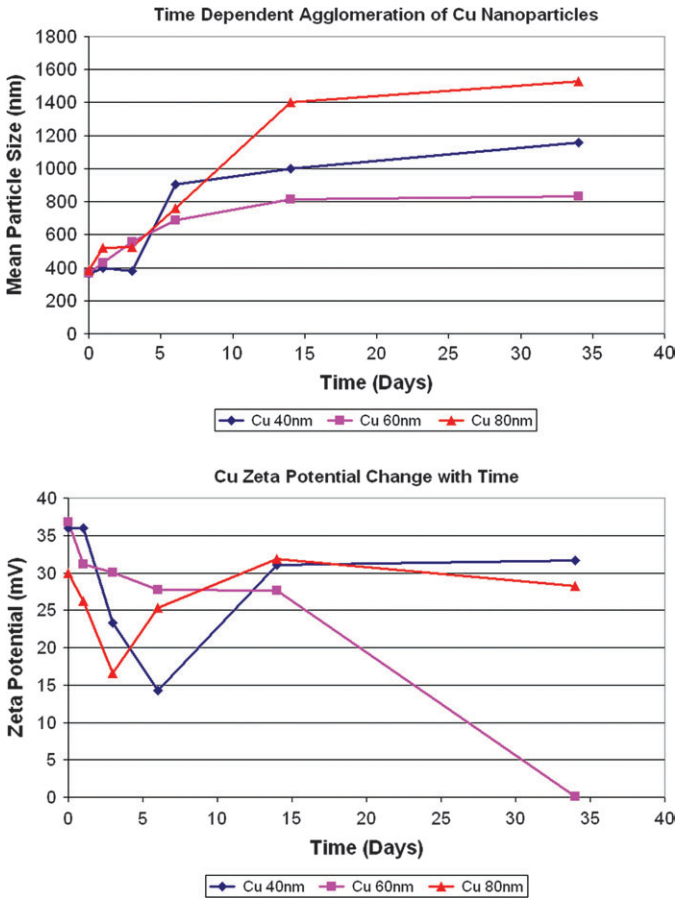

FIG. 10. Study of particle size and zeta potential for Cu 40, 60, and 80 nm stock solutions over a 34-day period. (A) Increasing mean particle/agglomerate size over 34 days for Cu 40, 60, and 80 nm 1 mg/ml stock solutions. (B) Fluctuating zeta potential values over 34 days for Cu 40, 60, and 80 nm 1 mg/ml stock solutions.

The zeta potential values appear to be correct but will most likely change significantly once placed in a different solution, such as ethanol. CB was analyzed in various solutions; however, no obvious trend of agglomeration arose from the data collected.

After studying the data gathered from many trials of sample sonication, it was determined that, at least with the silver samples tested, probe sonication can help disperse materials in solution better and obtain a more homogeneous mixture. However, the particles are still not readily dispersed at or near their primary particle size. Sonication did not seem to have a significant effect on the zeta potential of the particles, and therefore, it can be concluded that the particles would be just as likely to agglomerate again after a period of time. As seen in both the PS-Ag 25–30 nm and HC-Ag 25 nm particles, any increased sonication either lowered or did not affect their zeta potential. Decreasing the zeta potential of a particle could cause it to agglomerate even more since there is not as strong a repelling force between the particles as before. Short periods of sonication, 10–30 s, seem to have the largest impact on zeta potential as seen with the PS-Ag 25–30 nm sample. With the PS-Ag 25–30 nm particles, the particles are coated in a polysaccharide compound to aid in initial dispersion. It has been concluded that the sonication may affect this coating, most likely by removing some or all of it and therefore impact the surface charge of the particle and the state of dispersion in general. The probe sonication method can aid in temporarily suspending material in solution but does neither significantly reduce agglomeration nor provide a lasting, stable suspension of particles. Also, cytotoxicity assays were previously conducted with the HC-Ag 25 nm and PS-Ag 25–30 nm particles on rat neuroblastoma cells (N2A) with a nonsonication dose and a 60-s sonication dose. These experiments showed that the HC-Ag 25 nm solution that was sonicated for 60 s was only slightly more toxic, even at 50–100 μg/ml concentrations, when compared to the nonsonicated sample (unpublished data, Schrand, A.). The PS-Ag 25–30 nm exhibited no difference in toxicity between nonsonicated and sonicated samples.

Analysis of the Cu stock solutions over a 34-day time period yielded increased particle agglomeration and fluctuating zeta potentials. Each of the Cu solutions, Cu 40, 60, and 80 nm, were initially at similar agglomerate sizes, approximately 380 nm. As time increased, each solution produced larger agglomerates with the trend being logarithmic in nature. After approximately 30 days, Cu 40 nm increased to 1150 nm, Cu 60 nm increased to 820 nm, and Cu 80 increased to 1510 nm. This experiment also demonstrated that particles in solution can change surface energy over time and impact their dispersion in a stock solution, with each particle's zeta potential fluctuating over the 34-day time period. It is unclear why the zeta potential for Cu 60 nm decreased to near 1 mV after 34 days; however, it was observed that the particles were more agglomerated and settled more rapidly than earlier measurements conducted. The Cu particles also changed morphology under TEM imaging

after the 30-day time period. In dry form and after initial dispersion in water, the Cu particles appear to be spherical in nature; however, after time in solution, the particles' morphology changed from spherical to a more crystalline form. The center of the particle was still spherical, but with reduced diameter, and crystalline "spikes" protruded from the surface. This indicates dissolution of the Cu into the water (Cu^+ ions), which would have a significant impact on zeta potential of the particles. Upon repetition of this experiment, cytotoxicity assays would be conducted at similar timepoints to determine the extent to which these fluctuations in particle characteristics impact *in vitro* toxicity.

A final observation to be made from these experiments is that it is absolutely necessary to confirm particle characteristics "in-house" prior to *in vitro* testing. It is not enough to accept analysis and characterization from the manufacturer. Primary particle size listed by the manufacturer is a mean size value and with a mean value is a size range associated to it. For example, not only did the Cu 60 nm particles have an average size of 80 nm but also the SD of this average was ± 21 nm. That is a very large range especially when attempting to determine size-dependent toxicity. Also, it was discovered that an additional dispersant had been used on the PS-Ag 10 nm sample through XPS analysis meaning that any toxicity effects seen could not purely be based on the polysaccharide coating alone. This was not known from the manufacturer until after the analysis was complete, and the manufacturer was contacted about the high Na and S readings.

In summary, the DLS results illustrate that depending on the material, once the nanomaterials are in solution they do not necessarily retain their "nano-size." With the exception of the silicon dioxide particles and the Ag 10 nm dispersed particles, all the other materials assayed have a tendency to form large agglomerates that fall above the 100 nm size, indicating that some property other than size is playing a role in the toxicity of the material. This includes particle interaction with serum proteins, which was observed to have a significant effect on particle dispersion for certain materials. This study demonstrates the critical need to not only characterize materials when received but also how nanomaterials respond in solution prior to considering their uses in toxicity studies and how toxicity data may be significantly affected by these differences. While this study demonstrates how dispersion effects nanomaterials prior to dosing, researchers will still need to take into account how the cellular environment will impact nanoproperties once a cell or organism has been dosed. Therefore, there is also a need to further characterize nanomaterials once the material has been in contact with and/or taken up by a cell.

FUNDING

Biosciences and Protection Division, Human Effectiveness Directorate, Air Force Research Laboratory under the Oak Ridge Institute for Science and Education (to R.C.M. and A.M.S.). Postdoctoral Fellowship through the National Research Council (to L.B.-S.). In part by an appointment to the Student Research Participation Program at the U.S. Air Force Research Laboratory, administered by the Oak Ridge Institute for Science and Education through an interagency agreement between the U.S. Department of Energy and the USAFRL. Air Force Office of Scientific Research Project (JON # 2312A214).

ACKNOWLEDGMENTS

The authors would like to thank Col J. Riddle for his strong support and encouragement for this research. The authors would also like to recognize Mr Scott Streiker at the Nanoscale Engineering Science and Technology Laboratory, University of Dayton for his helpfulness with the HR-TEM.

REFERENCES

Berne, B. J., and Pecora, R. (1975). *Dynamic Light Scattering*. John Wiley, New York.

Bucher, J., Masten, S., Moudgil, B., Powers, K., Roberts, S., and Walker, N. (2004). Developing experimental approaches for the evaluation of toxicological interactions of nanoscale materials. Final Workshop Report 3–4 November. 2004, pp. 1–37. University of Florida, Gainesville, FL.

Dai, L. (2005). Low temperature, controlled synthesis of carbon nanotubes. *Small*. **1,** 274–276.

Gao, F., Wang, L., Tang, L., and Zhu, C. (2005). A novel nano-sensor based on rhodamine-*b*-isothiocyanate—Doped silica nanoparticle for pH measurement. *Mikrochim. Acta* **152,** 131–135.

Hood, E. (2004). Nanotechnology: Looking as we leap. *Environ. Health Perspect.* **112,** A740–A749.

Hussain, S., Javorina, A., Schrand, A., Duhart, H., Ali, S., and Schlager, J. (2006). The interaction of manganese nanoparticles with PC-12 cells induces dopamine depletion. *Toxicol. Sci.* **92,** 456–463.

Kim, D., Zhang, Y., Voit, W., Rao, K., Kehr, J., Bjelke, B., and Muhammed, M. (2001). Superparamagnetic iron oxide nanoparticles for bio-medical applications. *Scripta Mater* **44,** 1713–1717.

Kimbrell, G. (2006). Nanomaterials in personal care products and FDA regulation. The International Center for Technology Assessment. Available at: www.icta.org/doc/HBA_NYC_9_06_Nano_in_Personal_Care_Products.pdf. 13 September 2006.

Lee, M., Lee, G., Park, S., Ju, C., Lim, K., and Hong, S. (2005). Synthesis of TiO2/SiO2 nanoparticles in a water-in-carbon-dioxide microemulsion and their photocatalytic activity. *Res. Chem. Intermed.* **31,** 379–389.

Malvern Instruments Ltd. (2005). *Zetasizer Nano Series User Manual. MAN0317 Issue 2.2*. Worcestershire, UK.

Müller, R. (1996). *Zetapotential und Partikeladung in der Laborpraxis*. Wissenschaftliche Verlagsgesellschaft mbH, Stuttgart, Germany.

Murugan, R., and Ramakrishna, S. (2005). Development of nanocomposites for bone grafting. *Composites Sci. Technol.* **65,** 2385–2406.

Oberdorster, G., Maynard, A., Donaldson, K., Castranova, V., Fitzpatrick, J., Ausman, K., Carter, J., Karn, B., Kreyling, W., Lai, D., *et al*. (2005a). Principles for characterizing the potential human health effects from exposure to nanomaterials: Elements of a screening strategy. *Part. Fibre Toxicol.* **2,** 8.

Oberdorster, G., Oberdorster, E., and Oberdorster, J. (2005b). Nanotoxicology: An emerging discipline evolving from studies of ultrafine particles. *Environ. Health Perspect.* **113,** 823–839.

Powers, K., Brown, S., Krishna, V., Wasdo, S., Moudgil, B., and Roberts, S. (2006). Research strategies for safety evaluation of nanomaterials. Part VI. Characterization of nanoscale particles for toxicological evaluation. *Toxicol. Sci.* **90,** 296–303.

Ringer, S., and Ratinac, K. (2004). On the role of characterization in the design of interfaces in nanoscale materials technology. *Microsc. Microanal.* **10,** 324–335.

The Royal Society. (2004). *Nanoscience and Nanotechnologies: Opportunities and Uncertainties.* RS Policy document 19/04.

Simakov, S., and Tsur, Y. (2006). Surface stabilization of nano-sized titanium dioxide: improving the colloidal stability and the sintering morphology. *J. Nanoparticle Res.*

Sinha, V., and Trehan, A. (2003). Biodegradable microspheres for protein delivery. *J. Control. Release* **90,** 261–280.

Skebo, J., Grabinski, C., Schrand, A., Schlager, J., and Hussain, S. (2007). Assessment of metal nanoparticle agglomeration, uptake, and interaction using high-illumination system. *Int. J. Toxicol.* **26,** 135–141.

Sondi, I., Goia, D., and Matijevic, E. (2003). Preparation of highly concentrated stable dispersions of uniform silver nanoparticles. *J. Colloid Interface Sci.* **260,** 75–81.

Wagner, A., Bleckmann, C., Murdock, R., Schrand, A., Schlager, J., and Hussain, S. (2007). Cellular interaction of different forms of aluminum nanoparticles in rat alveolar macrophages. *J. Phys. Chem. B* **111,** 7353–7359.

Wallace, W., Keane, M., Murray, D., Chisholm, W., Maynard, A., and Ong, T. (2007). Phospholipid lung surfactant and nanoparticle surface toxicity: Lessons from diesel soots and silicate dusts. *J. Nanoparticle Res.* **9,** 23–28.

Williams, D., Ehrman, S., and Holoman, T. (2006). Evaluation of the microbial growth response to inorganic nanoparticles. *J. Nanobiotechnology.* **4**.

Wu, Y., Yang, W., Wang, C., Hu, J., and Fu, S. (2005). Chitosan Nanoparticles as a novel delivery system for ammonium glycyrrhizinate. *Int. J. Pharm.* **295,** 235–245.